The UW-PTMS: Systematic studies, measurement progress, and future improvements

Robert S. Van Dyck Jr.*, David B. Pinegar, Seth Van Liew[1], Steven L. Zafonte

University of Washington, Physics Department, Box 351560, Seattle, WA 98195-1560, USA

Abstract

The UW-Penning trap mass spectrometer (UW-PTMS) is now able to generate measurements with uncertainties near 10 ppt, making it necessary to address several major systematics, both experimentally and theoretically, in order to improve our present accuracy. These effects range from the image charge shift, originally investigated two decades ago, to the recently investigated limits due to residual magnetron energy. Using the knowledge gained from these studies, the atomic mass of ^{16}O has been completely reviewed and the results of this re-analysis are presented. There is also an adjustment given for the atomic mass of ^{4}He and we present a preliminary result for the atomic mass of ^{2}H. In addition, we present our plans for replacing the present spectrometer with a new one containing a cylindrical storage trap that will be loaded using an external ion source and two hyperbolic traps whose dimensions are identical to the Penning trap in our present spectrometer. Thus, it is expected that the new spectrometer will have essentially the same systematics as those described in this paper.
© 2006 Elsevier B.V. All rights reserved.

PACS: 07.75+h; 32.10.Bi; 41.75.Ak; 82.80.Qx

Keywords: Penning-trap; Mass spectrometer; Cyclotron-frequency systematics; Atomic masses; Oxygen

1. Historical introduction

The illustrious history of single particle mass measurements began almost as an after-thought. After many hours of painstaking effort one evening in 1979, a single positron had finally been isolated in the Penning-trap spectrometer used for measuring the lepton's magnetic moment. The trap was located inside a superconducting solenoid, housed in a refrigerated cryostat. On that evening, the refrigeration failed, and the cyclotron resonances that were being taken on the single positron were going to be wasted, unless we calibrated the positron resonances using an easily loaded single electron. As a result, the first recorded single-particle mass comparison was made that night with a precision of 100 ppb [1].

In 1986, the isolation of a single proton was reported [2] and a year or two later, the first Penning-trap mass measurement on the atomic mass of the proton was completed at the 3 ppb level of accuracy (and reported at the 1988 "Frequency Standards and Metrology" Conference in Ancona, Italy [3]). Very shortly after that, the MIT Penning-trap mass spectrometer (PTMS) made its first sub-ppb comparison of CO^+ with N_2^+ [4]. Since those early years, great progress has been made, and these spectrometers have been improved by more than two orders of magnitude. For instance, the UW spectrometer, with a magnet whose long-term drift is on the order of a few parts in 10^{12}/h [5], has produced nearly 0.01 ppb atomic mass measurements on ^{16}O [6] and ^{4}He [7]. In addition, the MIT-spectrometer group has developed a new technique for making mass doublet measurements on two simultaneously trapped ions at the sub-0.01 ppb level; in particular, the mass ratio of $^{14}N_2^+$ with $^{13}C_2H_2^+$ was made at the 0.007 ppb level of accuracy [8].

The future for still higher accuracy mass measurements using the Penning trap mass spectrometer looks hopeful, but an attempt must be made to understand all the systematic errors associated with this device. Thus, the bulk of this paper (see Section 3) will be devoted to describing in detail those known

* Corresponding author.
  E-mail addresses: vandyck@phys.washington.edu (R.S. Van Dyck Jr.), pinegar@u.washington.edu (D.B. Pinegar), svanl001@umaryland.edu (S. Van Liew), zafonte@u.washington.edu (S.L. Zafonte).
[1] Present address: University of Maryland Medical, Radiation Oncology Department, 22 S-Green Street, Baltimore, MD 21201, USA.

systematic errors that constrain the UW-PTMS. This paper will also re-visit the oxygen comparison which has been re-analyzed in Section 4 using the knowledge gained from this systematic investigation. Then in Section 5, we will note the change required for the atomic mass of ^{4}He and a preliminary result will be presented for a deuterium mass measurement that has great promise of achieving a 0.01 ppb accuracy. Finally in Section 6, we will describe our replacement spectrometer which will increase the versatility of this instrument to make high-accuracy mass measurements over a wide range of possible atomic species. But first, we will briefly describe the spectrometer and the nature of the data that are taken in this instrument, in order to fully appreciate the systematics described in Section 3.

2. Basic experiment

There are several papers on the UW-PTMS in the literature [5,9–11] describing many aspects of this spectrometer in extensive detail. Here, we outline just the basic operation in order that the subsequent descriptions of systematic shifts are coherent. A five-electrode Penning trap (consisting of hyperbolic ring and end-caps with rotational symmetry around the magnetic field axis, plus two guard or compensation electrodes [12]) is used to isolate a single charged particle. Its motion along the symmetry axis can be excited by a very stable frequency synthesizer, causing current to be induced in the end-caps. One of these electrodes is used to observe this motion by means of an attached LC circuit, referenced to common ground. It is tuned to the axial frequency $\nu_z = (2\pi)^{-1}\sqrt{qV_0/md^2} \approx 3.5$ MHz, where V_0 is the ring to end-cap potential difference, $d = 0.211$ cm is the characteristic trap dimension (related to the separation between end-caps and the main ring-electrode radius), and q/m is the particle's charge-to-mass ratio.

The axial RF-drive is applied to the end-cap opposite the one used for detection and the resulting signal voltage is amplified by a custom-built, cryogenically cooled preamplifier and mixed with the original (appropriately phase-shifted) drive voltage to generate an error signal. If something happens to shift ν_z, the phase of the particle's motion changes so that the error signal becomes non-zero. This is then integrated to produce a correction voltage that moves the ring potential to a new value that again forces the error signal to zero. In this way, the charged particle's axial motion at ν_z is kept *frequency locked* to the stable drive synthesizer and the resulting correction voltage (now referred to as the "frequency-shift signal") gives real-time information about perturbative changes in the frequency of this easily observed resonance. It should be noted that when this shift is due to a direct excitation of one of the radial normal modes (at the observed cyclotron frequency ν_c' or the $\vec{E} \times \vec{B}$ magnetron drift frequency ν_m), the excited state does not quickly relax back to its initial equilibrium. Instead, they are induced to do so by the application of a non-uniform RF electric field at either $\nu_c' - \nu_z$ (referred to as the coupling drive) or $\nu_z - \nu_m$ (referred to as the cooling drive) [13].

The observation of the cyclotron resonance requires a coupling of the axial motion to the cyclotron orbit radius R_c or equivalently its energy E_c. For this purpose, the uniform magnetic field of strength $B_0 \approx 60$ kG (6 T) is given a residual quadratic B_2 term of about 0.6 G/cm^2 (0.6 T/m^2) which we can increase by a factor of two or four for the light ions. In addition, the guards can be adjusted to inject a small negative fourth-order term, C_4 [14], into the potential well. As a result, the first order perturbation theory [15,16] predicts that the unlocked axial frequency is coupled to the cyclotron normal mode as follows:

$$\frac{\delta\nu_z}{\nu_z} = \left(\frac{B_2}{2\alpha^2 B_0} - \frac{3C_4}{2d^2}\right) R_c^2 = \left(\frac{B_2 d^2}{B_0 q V_0} - \frac{3C_4 \alpha^2}{q V_0}\right) E_c \quad (1)$$

where $\alpha \equiv \nu_z/\nu_c'$. Fig. 1 gives an example of the detection response for a single ^{3}He^{2+} ion's cyclotron motion as it is swept through its resonance using an appropriate electric dipole field. For this light ion, the linewidth of the axial resonance is too small (typically ≤ 180 mHz) to allow a large C_4 term to provide the coupling. This is due to additional loss of signal-to-noise in the axial-frequency shift detector in competition with the intrinsic noise from the ring potential. Thus, the axial well is made as harmonic as possible and the magnetic coupling term is solely responsible for detecting ν_c'.

The characteristic behavior of the axial-frequency-shift signal in Fig. 1 depends on the sweep direction because of the relativistic mass increase of the particle as energy is absorbed into the radial motion. The down-sweep reaches a corner and becomes a straight line, indicating that the cyclotron frequency remains just slightly in front of the down-swept drive (assuming a sufficiently slow sweep). The up-sweep response is a step function (filtered through the response time of the feedback system) because the resonant cyclotron frequency is pulled through the drive frequency. On occasion, a clear ringing can be observed between the free and driven motions. In the above example, the long detection time-constant leaves only a faint beat note.

Such pairs of sweeps (as shown in Fig. 1) serve to bracket the cyclotron resonance and generate an observation of ν_c' at a particular instant in time. When combined with ν_z and ν_m, each bracketed pair can generate a measurement of the free-space cyclotron frequency (as described in Section 3.1) at the instant in time given by the average of the two corresponding corner times.
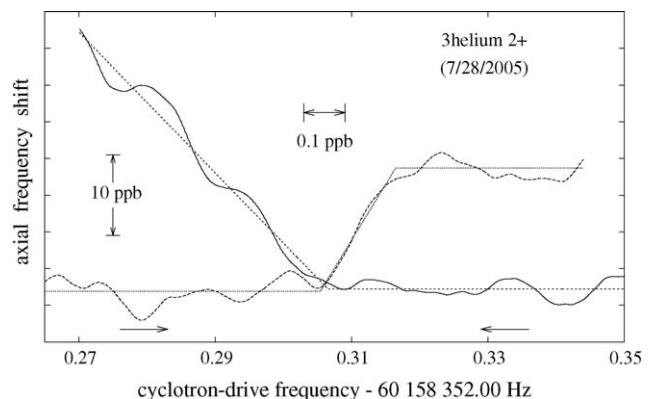

Fig. 1. The bracketed cyclotron resonance for a single ^{3}He^{2+} ion using our extrapolated triggered anharmonic detection method. The superimposed straight line segments are least-squares fitted lines and the typical "linewidth" (between corner frequencies) is 0.1–0.2 ppb. Also, the typical sweep time for each direction is 200–400 s.

Then, using several hundred such observations taken over 5–7 days, one can characterize the magnetic field drift for the ion of interest. By repeating this process immediately after replacing the original ion in the trap with the calibration ion, one can then scale both time records by the least-squares-fitted cyclotron frequency ratio (CFR), given by

$$\text{CFR} = \frac{\nu_c(\text{ion of interest})}{\nu_c(\text{calibration ion})}, \tag{2}$$

that now yields the best common drift record for both sets of data. The atomic mass of the ion of interest is determined from this CFR.

3. Systematic effects investigated for the UW-PTMS

The more one works to achieve greater accuracy in any research endeavor, the more one struggles to uncover hidden systematics. Thus, this section will describe those effects that have been considered up to this point. The Subsections 3.1–3.5 represent effects that could seriously affect the results of this mass spectrometer. These are then followed by Subsections 3.6–3.8 which describe effects which are presently below our level of sensitivity.

Early in this research program, we observed an effect associated with the angle of tilt between the electric and magnetic axes. The residual impact of this effect will be discussed in Section 3.1 where we deduce the level of accuracy at which the normal mode frequencies must be measured in order to avoid an erroneous result. Historically, the next effect that was encountered in this research program was the dependence on the amount of charge carried by the trapped ion. This effect will be discussed in Section 3.5. As our accuracy continued to improve into the sub-ppb level, it became imperative that we investigate as many other possible systematic effects as possible. The first of these (described in Section 3.2) is associated with the driven axial motion of the ion through the slightly inhomogeneous magnetic field and the non-quadratic electric field. We also became aware of the sensitivity of the cyclotron frequency to the phase of the axial drive, and this will be discussed in Section 3.3. In addition, we have determined that a systematic error even occurs due to the direction of the sweeps of the non-symmetric cyclotron resonance profile (see Section 3.4). The one dependence that was expected, but found to be negligible (see Section 3.6), is the dependence on the strength of the cyclotron drive. Also, the dependence on the magnetron energy has been of concern in the past and is discussed in Section 3.7. This dependence is expected to be negligible for all but the lightest ions (atomic number < 4). And lastly, there is some concern about the magnitude of a residual linear gradient in the magnetic field. This concern is shown to be unwarranted at the present level of accuracy in Section 3.8.

3.1. Shift due to angle and electrode asymmetry

In 1982, Brown and Gabrielse found that the observed normal-mode frequencies would all depend on the angle θ between the trap's electric axis and the direction of the magnetic field, as well as an electric asymmetry parameter ε [17]. Assum-

ing that $\nu_c = qB/2\pi m$ is the free-space cyclotron frequency and $\nu_c' + \nu_z^2/2\nu_c'$ is the previous estimate for ν_c, then the fractional shift between these two expressions is given by

$$\frac{\delta\nu_c}{\nu_c} = \frac{9\alpha^4\theta^2}{16} - \frac{\alpha^4\varepsilon^2}{8} \tag{3}$$

(where again $\alpha = \nu_z/\nu_c'$). In the early days of this research program, the angle θ was typically 0.01 rad (about 0.6°), and the trap electrodes associated with our first quadring trap [18] had a tolerance no better than 0.002 cm (a worst-case $\varepsilon \sim 1\%$) because of the difficulty in its fabrication. Thus, with typical values for α (0.06 < α < 0.1), the fractional shift in the cyclotron frequency is estimated to be 0.5–5 ppb. The present traps are machined to much better tolerances such that ε should be no larger than 0.1%. Likewise, the angle θ is carefully tuned to less than 0.001 rad. Thus, the corrections should be no worse than 50 ppt. However, that much error would still be intolerable with the kind of accuracy possible in these spectrometers. Fortunately, an exact prescription is available for determining the free-space cyclotron frequency by taking a quadrature sum of all the observable normal-mode frequencies [17]:

$$\nu_c^2 = (\nu_c')^2 + (\nu_z)^2 + (\nu_m)^2. \tag{4}$$

Because ν_c' is about an order of magnitude greater than ν_z, which is about an order of magnitude greater than ν_m, this invariance equation indicates that only ν_c' needs to be measured to the highest precision. In fact, to get 10 ppt accuracies in the CFR, the fractional error in the axial frequency should be less than 0.5 ppb (about 2 mHz) and the fractional error in the magnetron frequency should be less than 0.2 ppm (about 30 mHz).

3.2. Shift due to axial drive

This effect was first reported in this research program when we published our last measurement of the proton's atomic mass in 1999 [19]. As an example of this dependence, see Fig. 2 which shows the shift in the cyclotron frequency for a single $^3\text{He}^{2+}$ ion versus the square of the axial-drive voltage with arbitrary reference. (The typical axial-drive energy during normal run-conditions is 5–10 meV.) From first-order perturbation theory [16] one can show that the fractional shift in the observed cyclotron frequency (when ν_z is held constant as described in Section 2) is given approximately by

$$\frac{\delta\nu_c'}{\nu_c'} = \left\{ \frac{B_2 d^2}{B_0} - \frac{3C_4\alpha^2}{2} \right\} \frac{E_z}{qV_0} \tag{5}$$

where E_z is the total axial energy of the driven motion. This shift will now be shown to be directly proportional to the square of the axial drive voltage and inversely proportional to the square of the detection tuned circuit's Q-factor. Since the parameters in the bracketed terms in the above equation are all constants for a given ion, we need only investigate E_z/qV_0.

A moving trapped charge in a Penning trap can be characterized as being electrically equivalent to a current of amplitude I in a *fictitious* ℓcr tuned circuit. Using this model, the peak amplitude of the RF-drive voltage across the Penning trap is

$V_{\mathrm{RF}} = IR$ where R is the parallel resistance of the real LCR tuned circuit used for detection of the axial motion. The energy that characterizes the axial motion is given by $E_z = \ell_1 I^2/2$ where ℓ_1 is the particle-dependent inductance of the fictitious tuned circuit. The capacitive reactance of the real tuned circuit is $(\omega_z C)^{-1} = R/Q$, where C is the capacitance of the real tuned circuit and $Q \sim 1200$ represents the fractional energy lost per cycle in that circuit. Thus, it can be shown that

$$\frac{E_z}{qV_0} = \frac{\ell_1 C^2}{2md^2} \frac{V_{\mathrm{RF}}^2}{Q^2} \tag{6}$$

and the fractional shift in the observed cyclotron frequency becomes

$$\frac{\delta \nu_{\mathrm{c}}'}{\nu_{\mathrm{c}}'} = \{aB_2 - bC_4\} \frac{V_{\mathrm{RF}}^2}{Q^2} \tag{7}$$

where the constants are $a = (\ell_1 C^2)/(2mB_0)$ and $b = (3\alpha^2 \ell_1 C^2)/(4md^2)$. The nature of this model is readily apparent. The shift is seen to be dependent on the anharmonic terms, B_2 and C_4, as expected, but also inversely proportional to the square of the tuned-circuit Q-factor. When only the drive voltage is varied, the shift is indeed linear in the power of the axial drive (as shown in Fig. 2) and the residual effect of this systematic can be determined to better than 10 ppt in most cases. Other aspects of this model could not be checked at this time because it was noted that some components of the heterodyne (100 kHz sideband) axial drive system [20] have been varied over the last 6 years on several occasions, making it difficult to make accurate comparisons between ions of different runs. We plan to rectify this situation and make a systematic study of this model in the near future.

3.3. Shift due to axial-phase error

Several years ago, we noted [6] another source of error in the determination of the ion's cyclotron resonance frequency. It is associated with the phase of the axial drive, which is set as close as possible to the same phase as the reference in the phase-sensitive detector. This reference is mixed with the driven signal in order to shift it down to dc. When the phase is chosen prop-
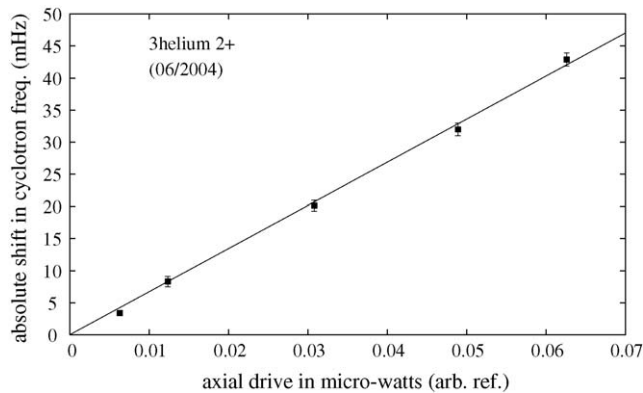

Fig. 2. The absolute shift in the observed cyclotron frequency is measured vs. power of the RF-drive applied to the axial motion of a single $^3\mathrm{He}^{2+}$ ion. The fitted line has a slope of 672 (15) mHz/μW(arb. ref.)

erly, the error signal alluded to in Section 2 (which establishes the frequency-lock for the axial resonance) is zero when the frequency of the drive oscillator is at the true axial resonance, ν_z. It then has the characteristic dispersion which is antisymmetric around zero.

It is relatively easy to show that if this phase is set incorrectly by an amount $\delta\phi$, then the error signal is proportional to $\sin(\delta\phi + \beta)$ where β is the phase-shift associated with a driven simple-harmonic oscillator whose drive frequency ω is not exactly on resonance. This quantity is found to equal $\tan^{-1}\{(\omega_z^2 - \omega^2)/\Delta\omega_z\omega\}$, where $\Delta\omega_z$ is the axial linewidth $2\pi\Delta\nu_z$. Since $\omega_z \gg \Delta\omega_z/2$ by many orders of magnitude, a linearized version can be obtained by defining $\omega \equiv \omega_z - \epsilon(\Delta\omega_z/2)$ where ϵ is the frequency offset in half-linewidths. The quantity β now equals $\tan^{-1}\{\epsilon\}$ and this can be approximated for $\epsilon < 0.17$ to yield $\beta = \epsilon$ to better than 1%. It follows that the error signal is now proportional to $\sin(\delta\phi + \epsilon)$, and when the lock-loop forces this quantity to zero, then $\delta\phi = -\epsilon$. Since $\epsilon = (\omega_z - \omega)(2/\Delta\omega_z) = \delta\omega_z(2/\Delta\omega_z)$, it follows that the shift in the axial frequency $\delta\omega_z$ becomes $-(\Delta\omega_z/2)\delta\phi$. Upon changing from radians to degrees, we obtain:

$$\delta\nu_z = -[0.00873/\mathrm{degree}]\Delta\nu_z\delta\phi \tag{8}$$

where $\delta\phi$ is the phase-error.

To get the shift in the calculated cyclotron frequency, one uses the invariance relation to obtain

$$\nu_{\mathrm{c}}(\mathrm{corr}) \approx \nu_{\mathrm{c}}(\mathrm{calc}) + \left(\frac{\nu_z}{\nu_{\mathrm{c}}}\right)\delta\nu_z \tag{9}$$

which then yields:

$$\frac{\delta\nu_{\mathrm{c}}}{\nu_{\mathrm{c}}} = -\frac{\nu_z}{\nu_{\mathrm{c}}^2}[0.00873/\mathrm{degree}]\Delta\nu_z\delta\phi. \tag{10}$$

To see if this relation agrees with experimental data, the frequency of the cyclotron resonance was measured for various deliberate phase errors, from $+30°$ to $-30°$ for a single carbon 6+ ion, as shown in Fig. 3. The error in the $\pm30°$ data points tends to approach 10% because the error in the approximation that $\beta = \epsilon$ is approaching 10%. The axial linewidth $\Delta\nu_z$ can be determined to better than 10% by using several theoretical fits to the observed axial-drive profile. In this case, this procedure yields $\Delta\nu_z = 488(45)$ mHz. Thus from Eq. 10, we obtained the theoretical slope for the line in Fig. 3 to be $-0.334(31)$ mHz/degree. This is in excellent agreement with the experimental value of $-0.367(10)$ mHz/degree.

3.4. Shift due to range of fitted sweep

A computer algorithm determines the center of the cyclotron resonance based on the axial-frequency-shift signal (described in Section 2) fitted over the whole RF-drive sweep (as shown by dotted lines in Fig. 1). Fig. 4 illustrates the systematic shift in ν_{c}' which is observed to be proportional to the range of sweep of the RF-drive oscillator. All ions investigated so far lie on the *same* straight line whose slope = 0.0291(9). This effect is believed to be related to the asymmetry of the ν_{c}'-resonance profile which is clearly visible in Fig. 1. When the normal-mode energy in the cyclotron resonance increases, the cyclotron frequency is reduced
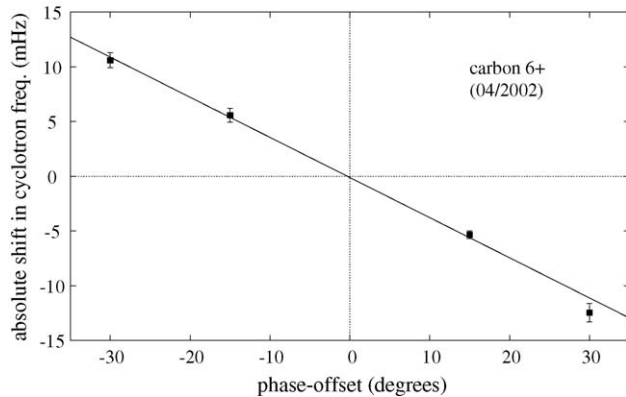
Fig. 3. The absolute shift in the observed cyclotron frequency is measured versus a deliberate phase offset for the RF-drive applied to the axial motion of a single C^{6+} ion. The fitted line has a slope of $-0.367(10)$ mHz/degree.
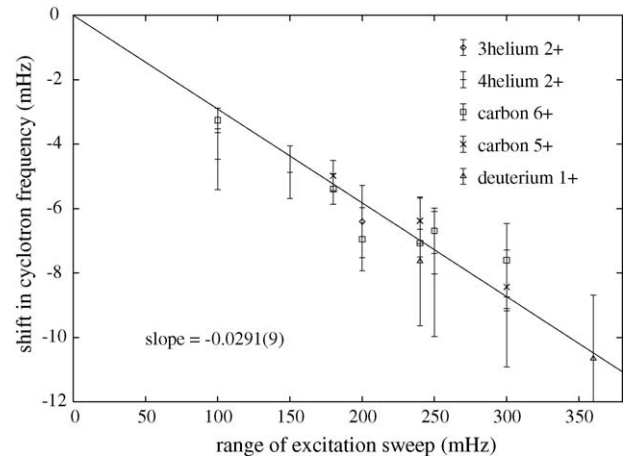

Fig. 4. The absolute shift in the observed cyclotron frequency is measured vs. various sweep ranges of the cyclotron drive synthesizer. Four species of ions were used to interrogate this shift, and in the case of carbon, two charge states were used. The slope of the fitted line is $-0.0291(9)$ mHz-shift/mHz-of-range, independent of the ion used. The sweep rate is kept constant for each ion being interrogated.

due to the relativistic increase in mass. Thus, in the down-sweep direction, the cyclotron resonance is pushed down in frequency with the sweep, assuming that the sweep rate is not too great. For instance, E_c will increase by 2 eV for a deuterium ion whose cyclotron resonance is pulled by about 50 mHz, which is the limit of a 100 mHz sweep (assuming the resonance was initially centered in the sweep range). On the other hand, the up-sweep direction pulls the resonant frequency through the drive, approximating a step function increase in the radial normal-mode energy. This increase can be as small as 0.3 eV, which is the amount that would cause the axial shift-signal of a deuterium ion to be equal to the noise in the detection circuit. This asymmetry has been investigated theoretically by at least two of the authors and one (SVL) is preparing a manuscript describing his work [21].

It has been suggested that the observed systematic shift is nothing more than a dependence on the rate of the RF-sweep. If this were so, then varying the time of sweep with a fixed range would be equivalent to varying the range with a fixed sweep time. This possibility was investigated several times, and each such test of varying the sweep-time (with fixed range) yielded a shift that was smaller than the uncertainty in the measurement. As an example, the comparison was made for data swept twice as fast using a $^3He^{2+}$ ion and the shift was found to be $-0.72(93)$ mHz in one case and $+0.44(78)$ mHz in a second case. We even tried quadrupling the sweep rate and in that case we found a shift that was zero with an uncertainty of 10 ppt. The preliminary theoretical treatment [21] suggests that a possible sweep-rate systematic shift exists, but would be negligible at the present level of precision. Since the magnitude of the observed shift is independent of the ion being interrogated (as shown in Fig. 4) and thus independent of the actual cyclotron frequency, we strongly believe that the effect is an artifact of the fitting routine that brackets the resonant frequency using any two consecutive up- and down-sweeps.

3.5. Shift due to image-charges

The major systematic that was observed very early in this research program is associated with the number of ions within

the trap. In fact, it was widely accepted that any breakdown in ideal trap symmetry would lead to a cyclotron resonance which depends on the number of trapped ions [22–24]. However, this dependence does not result from space charge, unless the cloud contains dissimilar ions, because electrostatic interactions between like-ions in the cloud whose extent is small compared to the wavelength of the exciting RF-field do not shift or broaden the cyclotron or axial resonances [25]. Nevertheless, as we continued to make a more quadratic potential, we found that the systematic dependence on the amount of charge that existed on the trapped ion did not go away. In fact, using a trap half the size of our present trap, the shift was found to be $\delta_e = 18(3)$ mHz/elementary-charge e, independent of the species trapped. To see the origin of this shift, we investigated the model of a free charge located in a spherical conducting enclosure [9], and our prediction was in excellent agreement with the value predicted from this model. Since that time, a much more refined treatment has been developed by Porto [26] for the hyperbolic electrodes used in the MIT Penning trap mass spectrometer. Here, the author also applied his realistic model to our hyperbolic electrodes and found excellent agreement with our old result.

To experimentally determine δ_e, two new experiments were conducted in the year 2000, primarily because the level of accuracy had become limited by the uncertainty in this quantity. One experiment compared 24 (1) O^{6+} ions to a single O^{6+} ion. The second compared two C^{6+} ions to a single C^{6+} ion. We obtained a preliminary value of 2.3 (1) mHz/elementary-charge. In this paper, we have re-analyzed that older data (now listed in Table 1), in light of the improved understanding of the other systematics described above.

In comparing pairs of the same species in this table, one notes that all the listed systematic errors are in common for both ions in a pair. For instance, in the case of the phase-error shift, the systematic effect depends directly on the axial linewidth, which is equal to a common constant times the number of ions in the

Table 1
Summary of cyclotron-frequency shifts associated with the trapped ions, O^{6+} and C^{6+}, used in the most recent determination of the image-charge effect

Sample ion type	Number in sample	Image-charge shift	Phase-error shift	Range-fit shift	Axial-drive shift
O^{6+}	24 (1)	$-24\,(1)6\delta_e$	$-40.0\,(10.0)$	$-2.90\,(10)$	$+0.70\,(4)$
O^{6+}	1	$-6\delta_e$	$-40.0\,(10.0)/24\,(1)$	$-1.45\,(5)$	$+0.67\,(2)$
C^{6+}	2	$-2(6\delta_e)$	$+11.24\,(1.37)$	$-1.74\,(6)$	$+1.26\,(13)$
C^{6+}	1	$-6\delta_e$	$+11.24\,(1.37)/2$	$-1.74\,(6)$	$+1.59\,(16)$

All shifts are in given in 'mHz' units and δ_e represents the image-charge shift per elementary charge e.

cloud. In the case of the range-fit shift, the effect depends only on the range of the sweep. Even in the case of the axial drive shift, the coefficient of the drive-power shift theoretically scales as the inverse linewidth. For both ion species in the above table, the axial shift for the sample with more than one ion has been determined from the theoretical model. In addition, in the case of the two C^{6+} ions, the shift was also measured to be $+1.15(7)$ mHz, which is in excellent agreement with the inverse-number extrapolated value, 1.26 (13) mHz (shown in the Table 1). As a result, we used the model and both measured values to determine that the correlated difference between the axial systematic shifts for the C^{6+} ions is $+0.30(6)$ mHz.

For the oxygen comparison, we have measured a cyclotron-frequency shift = $-343.8(1.5)$ mHz going from 24 ions to a single ion, which should also equal

$$[1 - 24(1)]6\delta_e - 40.0(10.0)\left[1 - \frac{1}{24(1)}\right]\ \text{mHz}$$

$$-1.42(6)\,\text{mHz}. \tag{11}$$

From the above expression, it follows that $\delta_e = 2.203(118)$ mHz. However, from the carbon comparison, we observe a shift = $-8.20(52)$ mHz going from two ions to a single ion which should equal

$$-6\delta_e + \frac{11.24(1.37)}{2}\ \text{mHz} - 0.30(6)\,\text{mHz}. \tag{12}$$

Using this last expression, it follows that $\delta_e = 2.253(143)$ mHz. By properly combining these two results, we obtain an image-charge shift for this Penning trap equal to 2.23 (9) mHz/elementary charge e.

3.6. Shift due to cyclotron drive

The theoretical coupling limit associated with the $\nu_c' - \nu_z$ coupling drive (see Section 2) gives rise to a thermal-equilibrium cyclotron energy $E_c(\text{th})$ which is given by $(\nu_c'/\nu_z)E_z(\text{th}) \approx 13(4)$ meV for all of our ions of interest (except for the proton which has about twice this energy). From this $E_c(\text{th})$, it can be shown (again using first-order perturbation relations [15,16]) that the fractional shift in the cyclotron frequency (due primarily to the relativistic mass shift) is less than 10 ppt. This term has always been ignored as being negligible. However, there has always been a concern that the excited cyclotron energy, required to detect an axial shift above the detection-system noise ($E_c(\text{det})$ on the order of eV) would produce a significant shift in ν_c'. But it must also be noted that the frequency shift detection method relies on the fact that the expected fractional width of the observed cyclotron

resonances is quite small, typically about 10^{-11} (for all of our ions except protons) due to residual external magnetic noise and axial-frequency noise coupled into this radial mode. Thus, the cyclotron drive must be essentially right on the corresponding resonance frequency before appreciable energy can be absorbed. Sweeping with a very weak RF-drive reduces the error caused when the beating of the particle's motion with the drive triggers early energy absorption by the non-linear relativistic resonance.

To address this possibility during the past atomic mass measurement of oxygen [6], we compared single C^{6+} and C^{4+} ions and observed that the comparison yielded the expected atomic mass value of 12.0 U to within 7 (7) ppt. Then with the aid of the axial-locked first-order perturbation equations [16] for $\delta\nu_c/\nu_c$ versus E_c, one would predict a systematic shift *at least* 10 times larger, if the fractional error in the comparison were determined by $E_c(\text{det})$. Therefore, it follows that the critical cyclotron energy used in the said perturbation relations should be less than $E_c(\text{det})/10 \sim 0.1$ eV. To experimentally check this conclusion, we have occasionally increased the strength of our cyclotron drive by 3–10 dB for all of our ions of interest. The most obvious change is an increase in the 'width' of the resonance where the 'width' is defined as the difference between respective corner frequencies shown in the cyclotron resonances traces (see Fig. 1). The nominal 'width' is generally adjusted to zero by choosing the appropriate combination of cyclotron drive power and the rate of sweep of the resonance. However, signal-to-noise suffers too much to do this for the light ions with $A < 4$. Table 2 lists several of these comparisons and in each case, the shift is essentially zero, consistent with its uncertainty. In addition, Fig. 5 illustrates the case for the first two C^{6+} entries in Table 2 which show a 6 dB increase and a 3 dB decrease in strength relative to our nominal drive strength. From the extrapolation, we obtain a fractional shift of $-3.9(1.4)$ ppt (relative to our nominal drive). The same perturbation relations would then predict a critical cyclotron energy $E_c(\text{excite}) = 0.049(17)$ eV, consistent with our expectations.

3.7. Shift due to magnetron motion

In the last few years, our accuracy has begun to push the 10 ppt level, and so in this section we now revisit the possible shift in ν_c' due to the cooled-limit of the magnetron normal mode, by estimating the typical magnitude of E_m. This subject was visited briefly during the measurement of the proton [19]. In general, from the first order perturbation theory under axial-lock conditions [16], one can show that the magnetron frequency is given by

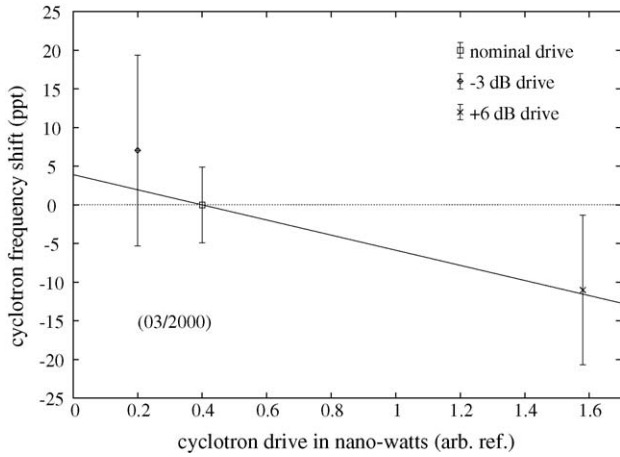$$\nu_m = \nu_m(0)\{1 + (aC_4)E_z + bE_z - (2aC_4)E_m\} \tag{13}$$

Fig. 5. The fractional shift in the observed cyclotron frequency of a single C^{6+} ion is determined for 6 dB more drive and 3 dB less drive. The very weak dependence on cyclotron power is dominated by the relativistic mass shift. In the present example, there is a negligible residual shift of < 0.004 ppb for the current nominal drive power.

where $a = 3/qV_0$ and $b = 3/4mc^2$. To be useful for high-precision measurements, one needs an axial linewidth that is large enough that the anharmonic line-broadening terms do not strongly effect the resolution of the axial frequency detector. Thus, C^{4+} was chosen over the proton because of its slightly larger linewidth and better signal-to-noise.

The magnetron frequency is actually obtained by observing the dip in the amplitude of the axial resonance as the cooling sideband is swept through $\nu_z + \nu_m$. However, in order for the constant terms in the above equation to disappear, the magnetron frequency is measured at symmetric extremes of $\pm5.6 \times 10^{-5}$ for the anharmonic coefficient C_4 and the difference between consecutive measurements of ν_m at these extremes are plotted versus axial drive power (see Fig. 6). Since the residual magnetron shift (= 0.17 (40) mHz when extrapolated to zero axial drive) is smaller than its uncertainty, we choose the residual shift in the above equation to be 0.4 mHz (with $\nu_m(0) = 0.21$ MHz). This extrapolation represents E_z becoming E_z(th) which is the un-driven axial energy established by the equilibrium of the free resonant motion with the detection amplifier near 4 K. For a C^{4+} ion, the quantity $2a|C_4|$ becomes about 1200 ppb/eV. Therefore,
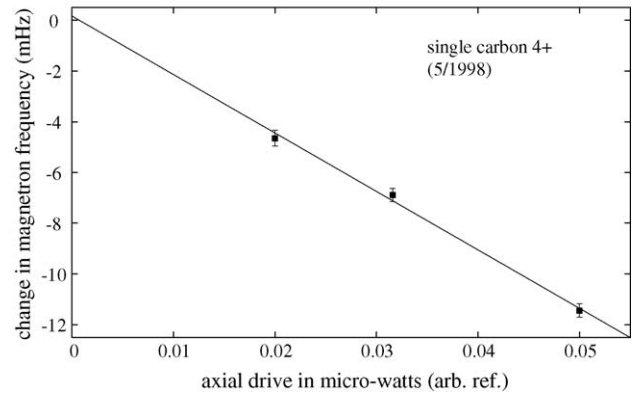

Fig. 6. The difference in magnetron frequency of a single C^{4+} ion is determined at symmetric extremes of $\pm5.6 \times 10^{-5}$ for the anharmonic C_4 coefficient vs. axial drive power. The solid line represents a linear fit to the data with an intercept = 0.17(40) mHz and a slope = $-231(13)$ mHz/μW.

it follows that:

$$E_z(\text{th}) + 2|E_m| \approx 1.6 \, \text{meV} \tag{14}$$

where the negative nature of E_m is explicitly shown [19]. Choosing the 4 K lower limit of 0.36 meV for E_z(th) requires $|E_m| < 0.6$ meV. However, if we use our best upper-limit estimate of 1 meV for E_z(th) [16] (due to the possibility that the amplifier which is coupled to the detection tuned circuit might induce noise that is warmer than ambient), we obtain a still lower limit 0.3 meV for $|E_m|$. On the other hand, the theoretical limit of the sideband cooled magnetron energy is $|E_m| = E_z(\text{th})\nu_m/\nu_z$ and if we again choose $E_z(\text{th}) = 1$ meV in the above relation, then $|E_m| = 0.06$ meV.

To see if the larger estimate of $|E_m|$ can produce a significant shift to the observed cyclotron resonance, we use the linear perturbation equations, again with the constraint of axial lock with constant ν_z:

$$\frac{\delta\nu_c'}{\nu_c'} = \frac{2B_2}{B_0}\left(\frac{c}{\omega_z}\right)^2 \frac{E_m}{mc^2} = \frac{E_m}{M} 40 \, \text{ppt} \tag{15}$$

where M is measured in proton masses, E_m is in units of eV, and again for our present spectrometer, $B_2 = 0.6$ G/cm^2, $B_0 = 60$ kG, with $\nu_z = 3.5$ MHz. Note that this expression does *not* depend on the charge of the ion, but does depend directly on

Table 2
Examples of measured shifts in the cyclotron frequency due to changes in the strength of the RF-drive power used to excite the cyclotron resonance

Sample ion type	Start of run	Nominal 'width' (mHz)	Power change (dB)	New 'width' (mHz)	Thermal 'bottle' width (mHz)	Observed resonance shift (mHz)
O^{6+}	6/20/1999	−0.1 (3)	+6	+6.5 (9)	<0.1	−0.12 (55)
C^{4+}	7/12/1999	−0.2 (4)	+6	+5.7 (1.2)	<0.1	−0.23 (61)
C^{6+}	3/7/2000	−1.6 (4)	−3	−8.3 (6)	<0.1	+0.32 (56)
C^{6+}	3/7/2000	−1.6 (4)	+6	+13.3 (6)	<0.1	−0.50 (44)
C^{6+}	12/19/2001	−4.6 (5)	+10	+9.3 (3)	<0.1	−0.54 (43)
$^2H^+$	12/31/2001	+20.5 (1.9)	+3	+35.1 (1.3)	∼ 0.4	−0.26 (1.37)
$^2H^+$	5/11/2003	+10.6 (1.0)	+6	+30.0 (1.5)	∼ 0.4	+0.35 (99)
$^2H^+$	12/8/2003	+11.4 (1.6)	+6	+45.0 (2.4)	∼ 0.4	+1.15 (1.70)
$^3He^{2+}$	8/17/2005	+24.1 (1.7)	+3	+49.8 (2.1)	∼ 0.4	+0.64 (1.51)

The 'width' is the difference between consecutive up-sweep and down-sweep corner frequencies shown in the cyclotron resonance traces. The column showing 'bottle' width corresponds to the axial thermal noise in the B_2 field gradient.

B_2. Thus, if $|E_m| = 0.6\,\text{meV}$, then the fractional shift in ν_c' is 24 ppt/M which is negligible for ^{4}He or larger masses. However, for our current research on ^{3}He, ^{2}H, and ^{3}H, the effect could be as large as 10 ppt. Since those species have small axial linewidths which can tolerate only small amounts of $C_4 < 2 \times 10^{-5}$, the B_2 term is required for coupling to the axial frequency detector. Therefore, it will be necessary to use at least three different values for B_2 and then extrapolate to zero gradient.

3.8. Shift due to magnetic gradients

By utilizing the axial-frequency shift detector, we can determine the dependence of the magnetic field on the ion's axial position. This is accomplished by using a small constant electric field in the axial direction obtained from a dc offset bias voltage ($\pm \Delta V$) asymmetrically applied to the two endcaps. This approximately linear steering field effectively shifts the equilibrium center-of-motion (to first-order) by an amount δ_z given by [15]

$$\frac{\delta_z}{d} = -\frac{C_1 d}{2Z_0} \frac{\Delta V}{V_0} \qquad (16)$$

where $2Z_0 = 0.456\,\text{cm}$ is the shortest distance between the endcaps and C_1 is the axial coupling constant, which is about 0.76 for our near-asymptotically symmetric trap configuration [15].

Upon measuring the cyclotron resonance versus axial position, and fitting the resulting data to a quadratic polynomial, we can determine both the linear and the quadratic gradients in the field. Also, we have three evenly-spaced solenoids wrapped around the vacuum envelop containing the Penning trap where the plane of the center coil coincides with the plane of symmetry of the ring electrode. Thus, we are able to generate both an additional linear and quadratic gradient when necessary. In particular, we routinely null the linear term to much less than 1 mG/cm, with an uncertainty over the last 10 years no worse than 0.7 mG/cm.

Next, we need to estimate the ion's center of oscillation relative to the geometrical center of the trap. We have two methods for doing this. First, when we drop the well depth to isolate a single ion, we know that we can get within 10's of millivolts above zero before losing the ion. Thus, in the extreme, we can assume that there is no more than 100 mV between endcaps. Using the above equation and assuming that $V_0 = 50\,\text{V}$, we deduce that the axial offset is no worse than 1.5 μm. The other method involves plotting out the ring potential required to keep the ion locked to the same axial frequency when varying the axial position described by the above equation. From the shifted quadratic dependence on potential, we are able to determine an axial offset that is typically 0.5 μm for the center-of-oscillation that has not exceeded 1.5 μm in the last 10 years. Thus, with a linear gradient no worse than 0.7 mG/cm and $B_0 = 60,000\,\text{G}$, the fraction shift for each ion is less than 2 ppt. For this amount of shift, we are confident that the systematic positional shift obtained by changing ions is negligible at our present level of accuracy. Of course, the effects of the quadratic gradient are already contained in the fractional cyclotron shift due to the axial drive as described in Section 3.2.

4. Re-analysis of oxygen atomic mass

The prime motivation for returning to the O^{6+} data came by way of a request from NIST [27] to use our value for the atomic mass of oxygen in conjunction with the measurement of the bound-state g-factor of the electron in hydrogen-like oxygen [28] in order to improve the value of the electron's atomic mass [29]. During a preliminary investigation, a few minor errors were discovered and it was noted that the data did not include the recently discovered 'range-fit' error (see Section 3.4). Thus, it was decided that a complete re-analysis should be undertaken, in which each run would be refitted. During this process, it was detected that one early run (second in the list of 10 shown in Table 1 of Ref. [6]) was unreliable (and would be dropped) because one key parameter that is used in the fitting process had been changed, but not recorded when the change occurred (near the beginning of the calibration stage).

Table 3 shows the list of shifts and their uncertainties associated with using C^{4+} as the calibration ion, while Table 4 lists similar data using C^{6+} as the calibration ion. Each run has an additional shift (not shown) of $-98.0(4.0)$ ppt due to the image-charge effect described in Section 3.5. As a result, a correction for this common shift has been applied to each run listed in these tables. However, the 4.0 ppt uncertainty must be added back in quadrature with the uncertainty in the weighted average of the nine remaining runs, since it is *not* an error that can be improved upon by taking more oxygen–carbon comparisons. One of the other improvements that has occurred since the majority of the oxygen runs were completed is that we have generated a fitting routine that allows the phase-offset to be estimated relative to the proper phase that should be set on the phase-sensitive detector. In most of these earlier runs, we simply estimated this phase (and its error) from the symmetry of the dispersion lineshape swept out on a xy-recorder. These estimates are reflected with the value '0' for the 'phase-offset' shift in all the runs except for the last few which did use the fitting routine. The 'range-fit' shift reflects our most recent determination shown in Section 3.4, and the effect turns out to be relatively small because some effort had been made to keep the corresponding ranges similar for both ions. This effect would actually cancel out if the two ranges had been scaled by their cyclotron frequencies.

We have estimated the CFR and its appropriate statistical error for each run in order to cover the distribution of multiple trial fits to the available data. Different trials correspond to parsing the data three or four times as if the run had been taken over consecutively smaller periods of time, centered on the transition to the calibration ion. For each parsing of the data, the basic time variation is assumed to be either strictly linear or containing a small quadratic dependence. In addition, some of the trials include a correction for the wander in ambient temperature or ambient pressure. In comparison to those shown in Table 1 of Ref. [6], the statistical errors have reduced in some cases and increased in others to reflect that the parsing is different from the original work. The combined uncertainty for each run, as reflected in the CFR-value given in the next to the last column, is obtained by taking all the listed contributions in quadrature, since *each* has been separately determined during each and every

Table 3
Oxygen runs using C^{4+} as calibration ion

Run start date	Statistical error	Axial drive shift	Axial drive error	Phase offset shift	Phase offset error	Range fit shift	Range fit error	Δ(CFR)	Δ(AM)
7/19/99	32.9	28.8	6.0	0	14.9	−3.3	0.1	495 (41)	18.96 (59)
8/07/99	14.2	7.3	4.4	0	13.1	−3.3	0.1	442 (22)	19.72 (32)
8/14/99	16.0	7.3	4.4	0	13.1	−3.3	0.1	439 (24)	19.76 (34)
9/22/99	15.1	−51.3	9.4	0	17.7	−3.3	0.1	539 (28)	18.35 (40)
Weighted	Mean							469 (24)	19.34 (34)

All shifts are in ppt (10^{-12}). In the next to the last column, Δ(CFR) = (CFR − 1.125383463000) × 10^{12}. In the last column, Δ(AM) = (atomic mass − 15, 994, 914, 600) in 10^{-9} U.

run. The value for the atomic mass, shown in the last column, is computed for each run by adding back the missing electrons and their binding energies. By taking the weighted average of atomic mass values for all nine runs together (each of which is shown separately in these two tables) and then combining in quadrature the resulting standard deviation of the mean with the 4.0 ppt error associated with the image charge shift, we obtain the following final value for the atomic mass of oxygen 16:

$$M(^{16}O) = 15, 994, 914, 619.57(18) \, nU. \qquad (17)$$

This new 11 ppt result agrees very well with the value reported in Ref. [6] (see note added in proof to that reference). It is quite conceivable that this atomic mass could be improved still further, since Table 4 shows significantly less scatter for the five runs using C^{6+} as the calibration ion than the four runs shown in Table 3 using C^{4+} for calibration.

It should be noted that the earlier reference to the bound-state g-factor measurements on O^{7+} was not limited by the present accuracy of our measurement of oxygen's atomic mass in the new determination of the electron's atomic mass [29]. However, the limitation to the accuracy of that experiment, which arises from the extrapolation of the axial temperature to 0 K, may disappear someday because of the use of novel phase-sensitive techniques recently developed by the Mainz-Darmstadt group [30].

5. Other atomic masses

First, the data recently published on the atomic mass of ^{4}He [7] is affected by the new result for the image-charge effect described in Section 3.5 and to a lesser extent by the change in the coefficient describing the range-effect shift given in Section 3.4. In fact, the average (positive) range correction to the CFR for the eight runs shown in that paper is only about −0.7 ppt

which is virtually negligible. However, the reduction in the net (negative) image-charge correction causes the CFR to increase by 6.1 ppt. Thus, the corrected weighted CFR for the 8 runs becomes 0.9993495023602 (134) and when the 7.9 ppt uncertainty associated with the image-charge correction is added in quadrature, we obtain the following value for the atomic mass of ^{4}He:

$$M(^4He) = 4, 002, 603, 254.131(62) \, nU \qquad (18)$$

where the change in this result represents a reduction in the atomic mass by about at third of the uncertainty.

As for the atomic mass of ^{3}He, we have only two runs completed at this point, and a third run in progress. Thus, it would be premature to list the details of those runs.

Finally, we have completed our investigation of the atomic mass of deuterium, with several runs having been taken between November 1999 and December 2002, all without the benefit of our new GPS-disciplined Rubidium standard. It had been observed in most of these older runs that the data would wander significantly on occasion without finding a correlation with any of the usual environmental parameters. Then, with the new standard as a reference, we discovered that our old crystal standard could wander about 100 ppt in as short a time as one day on some rare occasions, and typically about half that over several days.

Since the arrival of the new standard, we have made three or four additional runs with about half the previous uncertainty. This later research constitutes the thesis work of graduate student Steven Zafonte, and will be the basis of a future publication. However, we have carefully re-analyzed three of the most recent runs taken prior to the standard's arrival and they are listed in Table 5. The weighted mean of the three CFRs is 0.9929966546904 (699). The net image-charge correction that

Table 4
Oxygen runs using C^{6+} as calibration ion

Run start date	Statistical error	Axial drive shift	Axial drive error	Phase offset shift	Phase offset error	Range fit shift	Range fit error	Δ(CFR)	Δ(AM)
6/06/99	24.0	−0.8	11.0	0	10.8	0	0	88 (21)	20.07 (46)
3/04/00	26.7	15.5	3.2	0	7.9	2.2	0.1	110 (21)	19.60 (45)
4/03/00	25.3	−33.7	8.3	−49.9	20.4	8.6	0.3	109 (25)	19.62 (54)
5/02/00	14.7	21.3	5.5	0	15.4	8.6	0.3	112 (17)	19.55 (35)
7/06/00	10.7	6.7	1.1	−32.8	14.3	5.1	0.2	97 (13)	19.88 (29)
Weighted	Mean							102 (8)	19.76 (17)

All shifts are in ppt (10^{-12}). In the next to the last column, Δ(CFR) = (CFR − 0.750187093000) × 10^{12}. In the last column, Δ(AM) = (atomic mass − 15, 994, 914, 600) in 10^{-9} U.

Table 5
Deuterium runs taken in 2002 using C^{6+} as calibration ion

Run start date	Statistical error	Axial drive shift	Axial drive error	Phase offset shift	Phase offset error	Range fit shift	Range fit error	Δ(CFR)	Δ(AM)
1/26/02	21	−234	16.6	26	25.1	26	0.8	719 (36)	0.10 (7)
3/17/02	52	−131	7.6	12	29.5	46	1.4	820 (61)	−0.10 (12)
12/6/02	37	−156	5.3	−28	35.0	26	0.8	541 (51)	0.46 (10)
Weighted	Mean							690 (70)	0.16 (14)

All shifts represent corrections to the CFR in ppt (10^{-12}). In the next to the last column, Δ(CFR) = (CFR − 0.992996654000) × 10^{12}. In the last column, Δ(AM) = (atomic mass − 2, 014, 101, 778.000) in 10^{-9} U.

has been included in this result is −245 ppt. As usual, the uncertainty in the image-charge correction of 9.9 ppt is now included in quadrature to yield the following preliminary atomic mass for deuterium:

$$M(^2\text{H}) = 2, 014, 101, 778.161(143)\,\text{nU} \qquad (19)$$

which is accurate to about 70 ppt. As indicated above, the new runs should significantly reduce this uncertainty in the future. This result agrees well with our earlier 1995 published result [11] and the most recent result from MIT [31].

6. Future plans for a new spectrometer

In the early part of the 90's, the present apparatus was used with an enclosed (heated) titanium wafer containing some small fraction of a Curie of tritium. After several months, it was found that the trapped ions were giving very poor signal-to-noise in the locked axial resonance. Being suspicious of a source of ion contamination, we emptied the trap and put on positive potential for capturing electrons. After a weekend, a very large cloud (several hundred electrons) was discovered. We surmised that tritium gas had chemically bonded to the trap electrodes, and as it decayed, the escaping electron (with up to 18 keV of energy) was liberating gas adsorbed on the electrodes and subsequently ionizing some of it. The trap was disassembled and cleaned, but was never made entirely free of tritium. With a half-life of 12 years, this contamination has been a constant reminder of why one should not load radioactive tritium ions in this way.

After many years in planning, we are finally assembling a new spectrometer which is expected to extend the functionality of the system used to obtain the results reported here. While still taking advantage of most of our previously developed technology, we hope to make it easier to load ions of various desired species (such as tritium). With this new apparatus, it will be possible to reduce the measurement time (and at the same time improve our overall precision) since we should be able to shorten the time required to isolate a single ion of the desired species. And especially in the case of tritium, it is desirable to make the ion loading process as efficient as possible, in the sense that we want to minimize the amount of neutral tritium released into the trapping environment when we isolate this ion. In addition to reducing the time for switching between different ions, the precision double Penning-trap arrangement described below may allow us to make simultaneous measurements on two isolated ions, which offers intriguing possibilities for reducing some of our sources of systematic error.

There are two major differences between our present and future spectrometers. First, we have developed an external ion source and beam system, to ionize gas stored in cylinders, and then focus the ions into the cryogenic part of our new spectrometer. Fig. 7 is a schematic illustration of this new spectrometer. A dedicated computer will control a vacuum gate-valve, and a set of cylindrical electrodes whose potentials can be quickly switched. We can program a timing sequence that will momentarily allow beam current to flow into the strong-field region of our magnet, where ions will first be captured in a "storage tube" (which is in fact a crude Penning trap). The second important difference (illustrated in Fig. 8) is that below the storage tube, the new spectrometer makes use of *two* hyperbolic Penning traps. They are arranged along a common symmetry axis such that the lower ("experiment") trap is located in the most uniform region of the magnetic field (and contains a field-emission-point (FEP) electrode at its lowest point). The separation between the centers of the upper ("capture") trap and the lower ("experiment") trap is approximately 4.30 cm. By quickly pulsing down the voltages on the electrodes between any consecutive two of the three traps, we can transfer ions between them (similar to the way that positrons were transferred between traps in early g-2 experiments [32,33]).

Starting with perhaps 10^3 ions in the storage tube, it will be possible to apply a single pulse that is so fast that most of the ions will remain in the tube, but the timing can be adjusted such that a single ion is moved into the capture trap once every two to three pulses. The capture trap will be examined for an inhabitant after every pulse, and failing to find one, it will be dumped in case a contaminant ion has been loaded. This procedure will be repeated until we observe exactly one trapped ion-of-interest. As long as the ion beam contains perhaps 95% of the correct species, data obtained from such a procedure will have a very low probability of being contaminated. As a result, the possibility of losing signal-to-noise or, in the worst case causing frequency shifts, will be extremely remote.

One obvious use of the capture trap is to use it as a pre-trap which collects C^{6+} when the FEP is turned on. The trapped cloud can be cleaned in this trap and then one C^{6+} can be pulsed down into the experiment trap. Another possible usage of the double-trap configuration envisions having a single ion of species "A" in the top trap, and one of species "B" in the lower trap. Then, pulses are applied so that the two ions fly past each other between the traps, and are subsequently re-captured and quickly ready for measurement. This represents a very fast way to exchange the ion in the precision experiment trap. Although it may not be
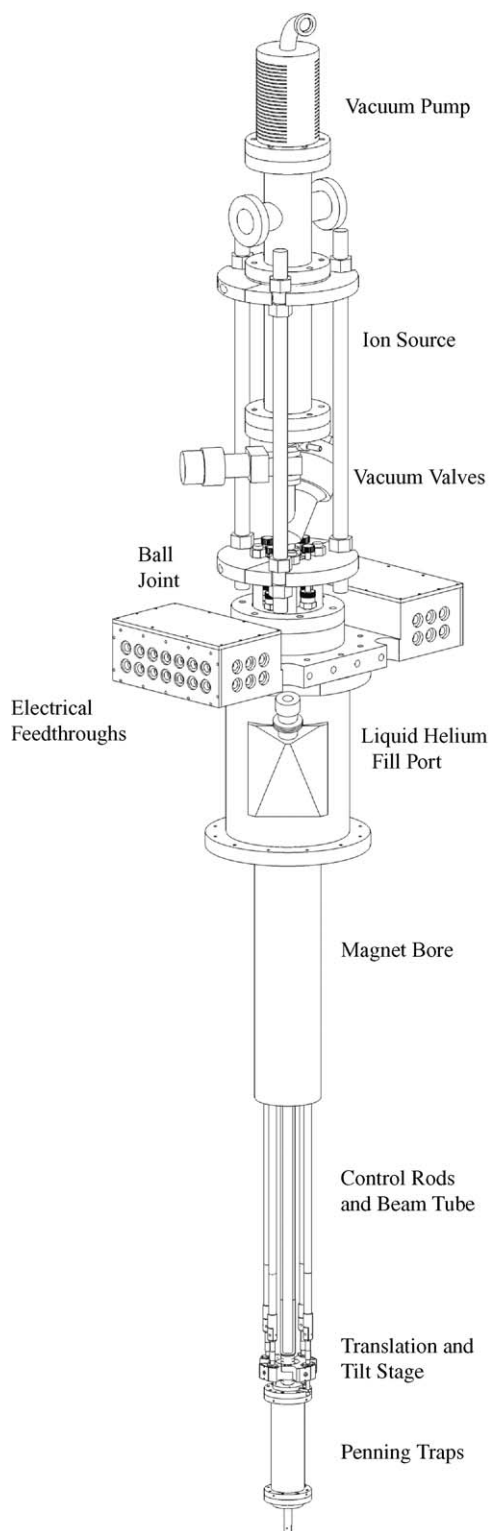
Fig. 7. External view showing the mechanical arrangement of the ion source, beam-tube, and Penning traps. The control rods and translation/tilt stage allow the location of the Penning traps to be adjusted by rotating knobs located just above the ball joint. The distance from the ion source to the experiment Penning trap is about 150 cm.
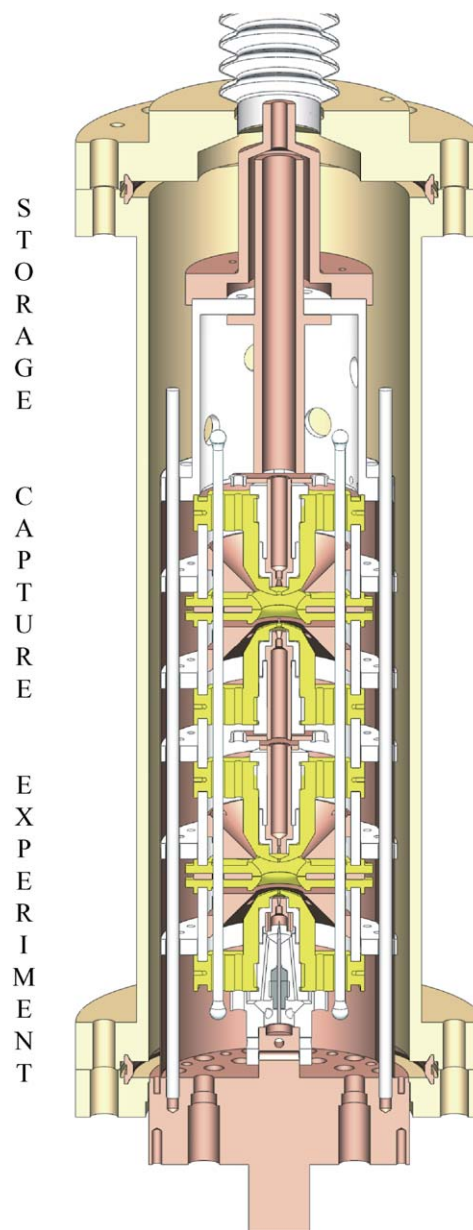

Fig. 8. Cross-sectional view of the aluminum–bronze vacuum envelope within which three new traps are shown. The cylindrical copper "ring" electrode of the storage trap (near the top where the beam enters) is 5.1 cm long. The phosphor–bronze capture and experiment traps are both identical to the hyperbolic Penning trap located in the present UW-PTMS (with characteristic dimension $d = 0.21$ cm). The one exception is the central holes in capture-trap end-caps which have a diameter of 0.51 mm (in comparison to those in the experiment trap with a diameter of 0.30 mm). The FEP electrode shown below the experiment trap can be used to alter the ionic charge state in either trap when necessary.

as elegant as the exchange of two ions between regions of *the same* trap, this method does have the advantage of eliminating any frequency shifts that depend on the distance separating two similar q/m ions. After all, an ion's cyclotron frequency is most easily measured when it is isolated at the center of a clean high-precision Penning trap.

Acknowledgement

References

[1] P.B. Schwinberg, R.S. Van Dyck Jr., H.G. Dehmelt, Phys. Lett. 81A (1981) 119.

[2] R.S. Van Dyck Jr., F.L. Moore, D.L. Farnham, P.B. Schwinberg, Bull. Am. Phys. Soc. 31 (1986) 974.

[3] R.S. Van Dyck Jr., F.L. Moore, D.L. Farnham, P.B. Schwinberg, A. De Marchi (Eds.), Frequency Standards and Metrology, Springer-Verlag, Berlin, Heidelberg, 1989, p. 349.

[4] E.A. Cornell, R.M. Weisskoff, K.R. Boyce, R.W. Flanagan Jr., G.P. Lafyatis, D.E. Pritchard, Phys. Rev. Lett. 63 (1989) 1674.

[5] R.S. Van Dyck Jr., D.L. Farnham, S.L. Zafonte, P.B. Schwinberg, Rev. Sci. Instrum. 70 (1999) 1665.

[6] R.S. Van Dyck Jr., S.L. Zafonte, P.B. Schwinberg, Hyperfine Interact. 132 (2001) 163.

[7] R.S. Van Dyck Jr., S.L. Zafonte, S. Van Liew, D.B. Pinegar, P.B. Schwinberg, Phys. Rev. Lett. 92 (2004) 220802/1.

[8] S. Rainville, J.K. Thompson, D.E. Pritchard, Science 303 (2004) 334.

[9] R.S. Van Dyck Jr., F.L. Moore, D.L. Farnham, P.B. Schwinberg, Phys. Rev. A 40 (1989) 6308.

[10] R.S. Van Dyck Jr., R. Hulet, B. Dunning (Eds.), Atomic, Molecular, and Optical Physics: Charged Particles, Vol. 29A of Series on Experimental Methods in the Physical Sciences, Academic Press, New York, 1995, p. 363.

[11] R.S. Van Dyck Jr., D.L. Farnham, P.B. Schwinberg, in: Proceedings of Nobel Symposium on 'Particle Traps and Related Fundamental Physics' in Lysekil, Sweden, Phys. Scr. T59, 1995 p. 134.

[12] R.S. Van Dyck Jr., D.J. Wineland, P.A. Ekstrom, H.G. Dehmelt, Appl. Phys. Lett. 28 (1976) 446.

[13] R.S. Van Dyck Jr., D.L. Farnham, P.B. Schwinberg, Physica Scripta 46 (1992) 257.

[14] G. Gabrielse, Phys. Rev. A 27 (1983) 2277.

[15] L.S. Brown, G. Gabrielse, Rev. Mod. Phys. 58 (1986) 233.

[16] D.L. Farnham, A Determination of the Proton/Electron Mass Ratio and the Electron's Atomic Mass via Penning Trap Mass Spectroscopy, PhD Thesis, University of Washington, Seattle, 1995.

[17] L. Brown, G. Gabrielse, Rapid Communications, Phys. Rev. A 25 (1982) 2423.

[18] R.S. Van Dyck Jr., P.B. Schwinberg, S.H. Bailey, J.A. Nolen Jr., W. Benenson (Eds.), Atomic Masses and Fundamental Constants 6, Plenum Press, New York, 1980, p. 173.

[19] R.S. Van Dyck Jr., D.L. Farnham, S.L. Zafonte, P.B. Schwinberg, Trapped Charged Particles and Fundamental Physics, AIP Conf. Proc. 457 (1999) 101.

[20] F.L. Moore, D.L. Farnham, P.B. Schwinberg, R.S. Van Dyck Jr., Nucl. Instrum. Methods Phys. Res. B 43 (1989) 425.

[21] S. Van Liew, An Ultra-Precise Determination of the Mass of ^{3}He using Penning Trap Mass Spectrometry, PhD Thesis, University of Washington, Seattle, 2004 (also, manuscript in preparation for Phys. Rev. A).

[22] S. Liebes Jr., P. Franken, Phys. Rev. 116 (1959) 633.

[23] G. Gärtner, E. Klempt, Z. Phys. A 287 (1978) 1.

[24] G. Gräff, H. Kalinowsky, J. Traut, Z. Phys. A 297 (1980) 35.

[25] D. Wineland, H. Dehmelt, Int. J. Mass Spectrom. Ion Proc. 16 (1973) 338.

[26] J.V. Porto, Phys. Rev. A 64 (2001) 023403/1.

[27] B. Taylor, National Institute for Standards and Technology, Private Communication, 2002.

[28] J. Verdú, T. Beier, S. Djekic, H. Häffner, H.-J. Kluge, W. Quint, T. Valensuela, G. Werth, Hyperfine Interact. 146/147 (2003) 47.

[29] J. Verdú, S. Djekic, S. Stahl, T. Valensuela, M. Vogel, G. Werth, T. Beier, H.-J. Kluge, W. Quint, Phys. Rev. Lett. 92 (2004) 093002/1.

[30] S. Stahl, J. Alonso, S. Djekic, H.-J. Kluge, W. Quint, J. Verdú, M. Vogel, G. Werth, J. Phys. B: At. Mol. Opt. Phys. 38 (2005) 297.

[31] V. Natarajan, K.R. Boyce, F. DiFilippo, D.E. Pritchard, Phys. Rev. Lett. 71 (1993) 1998.

[32] P.B. Schwinberg, A Technique for Catching Positrons in a Penning Trap via Radiation Damping, PhD Thesis, University of Washington, Seattle, 1979.

[33] P.B. Schwinberg, R.S. Van Dyck Jr., H.G. Dehmelt, Phys. Rev. Lett. 47 (1981) 1679.